Ablation-Products Radiation from Cones

WILLIAM C. DAVY,* ROGER A. CRAIG,* GARY T. CHAPMAN,† AND DALE L. COMPTON†
NASA Ames Research Center, Moffett Field, Calif.

Conical bodies with ablation heat shields have been proposed to reduce the total heating of vehicles entering planetary atmospheres at hyperbolic speeds. The radiant emission from the products of ablation constitutes a source of heat input into the body. This source of heating has previously been studied for blunt bodies (NASA TN D-1978), and ballistic-range data have been correlated by means of a boundary-layer analysis. In the present study, the correlation parameters derived from the blunt-body tests are combined with solutions of the boundary-layer equations for laminar flow with mass injection for cones. Predictions were thus made of the ablation-products radiation to be expected on cones. Tests of polyethylene and polycarbonate 30° half-angle cones have been conducted to test the predictions. It is found that the ablation-products radiation of the cone models is predicted within a factor of 2. It appears that the present approach may be used for other shapes.

Nomenclature

C = boundary-layer edge velocity gradient, sec^{-1}
c_p = total specific heat
E = radiant output per unit mass, w-g^{-1}
f = dimensionless stream function
g = ratio of local total enthalpy to edge total enthalpy
H = total enthalpy
h = static enthalpy
h_{eff} = effective heat of ablation, joules-g^{-1}
J = local radiative power, w-cm^{-3}
K = radiation constant, $w(cm)^{3\zeta}(g)^{-(\zeta+1)}(°K)^{-\xi}$
K_c = convective heat-transfer constant, w-$cm^{-3/2}$
k = total thermoconductivity
l = $\rho\mu/\rho_w\mu_w$, where μ is viscosity
$\dot{m}$ = mass injection rate per unit surface area, g-cm^{-2}-sec^{-1}
$\dot{Q}_a$ = total ablation-products radiative heating flux, w
$\dot{q}$ = local heating rate, w-cm^{-2}
Re = Reynolds number based on boundary-layer edge conditions and slant length
r = radius from line of symmetry to location x on surface, cm
Sc = Schmidt number
s = surface area, cm^2
T = temperature, °K
u = velocity in x direction, km-sec^{-1}
V = velocity, km-sec^{-1}
V_d = diffusion coefficient
v = velocity in y direction, km-sec^{-1}
W = mass fraction of ablation products in boundary layer
x = distance along surface, measured from cone apex, cm
y = distance measured normal to surface, cm
z = transformed normal distance, $\rho_w dz = \rho\, dy$
γ = transformed length
ζ = exponential dependence of E on density
η = transformed distance normal to wall
θ_c = half-angle of cone
ξ = exponential dependence of E on temperature
ρ = density, g-cm^{-3}
σ = Prandtl number

Subscripts

b = base
e = boundary-layer edge
w = wall
∞ = conditions at freestream
0 = standard sea-level conditions

Presented as Preprint 64-71 at the AIAA Aerospace Sciences Meeting, New York, January 20–22, 1964; revision received May 18, 1964.

* Research Scientist.
† Research Scientist. Member AIAA.

Introduction

IN the study of radiation associated with hypersonic flight, it has been noted in several papers[1–5] that the ablation process is accompanied by an increase in radiation from the vehicle shock layer. This increase is attributed[1] to ablation products in the boundary layer which have diffused outward from the surface and attained a high enough temperature to emit optical radiation. A more complete understanding of the process of ablation-products radiation is desirable and necessary because under certain conditions[1] this radiation can be a substantial part of the heating of vehicles entering the atmosphere. In addition, since the ablation process is intimately coupled with the energy exchange mechanism in the boundary layer, an understanding of the ablation-products radiation process may constitute a diagnostic tool for the study of atmospheric entry phenomena.

Recently, interest has been directed to conical shapes for atmospheric entry.[6] This interest arises from a need to reduce the over-all heating of a vehicle entering at hyperbolic speeds, at which the air radiation becomes excessive for a blunt vehicle. Since air radiation exhibits a strong temperature dependence, it is possible to reduce greatly the heating of the vehicle by air radiation by using a conical shape. Moderately increased convective heating is accepted for greatly reduced air radiation; however, not considered thus far is the heating on a cone due to ablation-products radiation, the presence of which may influence the minimization of total heating.

The purpose of the present paper is therefore to describe a method by which ablation-products radiation characteristics deduced from tests of blunt models in free-flight ballistic ranges can be used to predict ablation-products radiative heating on a cone. The predictions are arrived at through an analysis based upon an equation for the radiation per unit mass of ablated material. This equation assumes that for a given material there is a simple dependence of radiative power per unit mass on local values of temperature and density. The empirical constants in the equation describing this dependence are evaluated from computed boundary-layer properties on a blunt vehicle and from observations of ablation-products radiation during ballistic tests of blunt models. The resulting information is applied to the analysis of the boundary-layer properties on an ablating cone to correlate and predict the ablation-products radiation. The predictions are then compared with observations of ablation-products radiation in ballistic-range tests of cones.

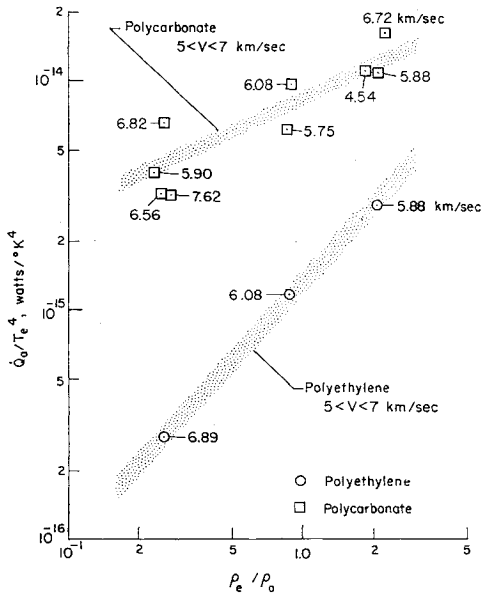

Fig. 1 Blunt-body data and correlating equation evaluated for velocities from 5 to 7 km/sec.

Analysis

The analysis by which the blunt-body ablation-products radiation was correlated, and which is extended to cones in the present paper, is based on a consideration of the gross processes that occur in the laminar boundary layer. The initial assumption is made that the ablation products are gases, ejected from the surface, which diffuse through the boundary layer. The radiant power output per unit mass of ablated material is assumed to have a power-law dependence on temperature and density given by

$$E = K\rho^{\zeta}T^{\xi} \tag{1}$$

where E is the power radiated per unit mass of ablated products, ρ and T are the total properties of the air-ablation products mixture, and the parameters K, ζ, and ξ are constants that depend only on ablation material. Note that any effects on ablation-products radiation due to chemistry (species change, etc.) will appear especially in the magnitude of ζ. A ζ value of zero, for example, removes the density dependence from Eq. (1), and this infers that if there are chemical reactions present they either do not change ablation-products radiation or are not density dependent.

A heating flux $\dot{Q}_a$ is defined as the total radiant power due to ablation-products radiation which is incident on the body surface. If the source is geometrically and optically a thin radiating boundary layer, then $\dot{Q}_a$ is obtained by integrating one-half the radiant power output from the boundary layer over the body surface, namely,

$$\dot{Q}_a = \frac{1}{2}\int_{\text{surface}}\int_0^{y_e} WE\rho\, dy\, ds \tag{2}$$

where W is the mass fraction of the ablation products in the boundary-layer mixture, ρ is the total gas density (air and ablation products), both being functions of y, the distance normal to the ablating surface. The integration limit y_e is defined as the smallest value of y beyond which contributions to the heating flux are negligible; in practice, y_e is taken as the value of y where W is 0.5% of the wall value.

Blunt-Body Analysis

The application of Eq. (2) to the boundary layer of a blunt body and the use of test data to evaluate the constants ζ, ξ, and K in Eq. (1) are described in detail in Ref. 1 and are briefly outlined below.

For blunt-body boundary layers, Eq. (2) may be integrated in closed form if several simplifying assumptions‡ are made. The most important of these are 1) that the velocity, temperature, and ablation-products mass fraction are linear functions of the transformed normal distance from the wall, z, defined by

$$\rho\, dy = \rho_w\, dz \tag{3}$$

2) that the variables all reach edge values at the same distance from the wall, and 3) that the mass injection rate of ablation products is constant over the ablating blunt face of the body. With these approximations and several other mathematical simplifications, Eq. (2) can be integrated in closed form to give

$$\dot{Q}_a = \frac{3sK\dot{m}\rho_e^{\zeta}T_e^{\xi+2}}{2C(\xi-\zeta+1)(\xi-\zeta+2)(T_e-T_w)^2} \tag{4}$$

where s is the surface area of the body face, $\dot{m}$ is the mass injection rate, and C is the edge velocity gradient parallel to the surface. Calculations of $\dot{Q}_a$ based on observations of ablation-products radiation from blunt models made of polycarbonate and polyethylene were correlated by use of Eq. (4) to obtain values of K and ζ. The approximate values so obtained are as follows: polycarbonate, $K = 7 \times 10^{-8}$, $\zeta = 0$; and polyethylene, $K = 6 \times 10^{-7}$, $\zeta = 0.66$. Evaluation of ξ from the polycarbonate data gave 3.5 ± 1, whereas insufficient variation of edge temperature for the polyethylene tests made meaningful determinations of ξ for polyethylene difficult. A value of 4.0 was used for convenience to correlate the data for both materials.

Figure 1 demonstrates how well the blunt-body data of Ref. 1 are correlated by Eq. (4) with the foregoing values of the parameters. The factor T_e^{-4} appropriate for $\xi = 4$ and $T_w \ll T_e$ was used to reduce velocity dependence and allow a concise presentation over the velocity range of the data. The shaded regions in the figure represent Eq. (4) evaluated for a velocity range of 5 to 7 km/sec. The figure shows that the equations correlate the data to an accuracy of approximately ±50%. The fact that polyethylene ablation-products radiation is more sensitive to changes in edge density is readily apparent, and this fact is reflected in the numerical magnitude of the density exponent. The reason the curves plotted in Fig. 1 do not exhibit slopes that compare with the value of ζ listed previously (e.g., the curve for polycarbonate does not have zero slope) is that terms in Eq. (4) other than ρ_e^{ζ} have implicit density dependencies. The mass injection rate $\dot{m}$ has a strong density dependence. For the test conditions, for example, convective heating was the primary energy source causing ablation; thus, the mass injection rate varies approximately as the square root of the boundary-layer-edge density.

Cone Analysis

To predict the ablation-products radiation from boundary layers on cone-shaped bodies, Eq. (2) must be integrated with the appropriate boundary-layer temperature, density, and ablation-products distributions, which are different from those on a blunt body. As will be shown, the distribution of temperature within the boundary layer on a conical body is so nonlinear that the simplifying linear approximations used in the blunt-body analysis can no longer be applied. To obtain the distributions of local values of temperature, concentration of ablation products, and density, it was necessary to solve by digital computer the differential equations for momentum, energy, and mass conservation in the boundary layer, with appropriate boundary values specified at the wall and at the

‡ The assumptions are based upon reasonable approximations of the boundary-layer processes on an ablating blunt body and are discussed in Ref. 1.

boundary-layer edge. The major assumptions that were used to obtain these solutions are as follows:

1) The boundary layer is thin (usual boundary-layer assumption[7]).

2) The injected material (ablation products) has the same state and transport properties as does equilibrium air, with, of course, the exception that its radiative property is given by Eq. (1).

3) The state and transport properties of the gas are given by the calculations of Hansen.[8] (Note: the total thermal conductivity is used as opposed to the partial conductivity.)

4) The radiative energy loss from the boundary layer is neglected (i.e., no radiative-convective coupling).

A description of the solutions of the boundary-layer equations for a cone is to be found in the Appendix. A typical set of boundary-layer profiles resulting from these solutions is shown in Fig. 2. The figure shows the variation of the boundary-layer temperature and ablation-products mass fraction with distance from the wall. Shown also are the same distributions for the blunt body, as calculated from the earlier blunt-body analysis.§ The calculations are based on the model configurations, 30° half-angle for the cone, and nose radius-to-diameter ratio of 0.71 for the blunt body. The freestream density and velocity are equal for both geometries. Note that the mass fraction distribution for both cases is nearly a linear function of distance from the wall. However, the temperature distributions are markedly different; the boundary layer of a cone is bounded by a much lower edge temperature and shows a small overshoot of this temperature within the layer.

The local value of the radiation in power per unit volume is given by the expression

$$J = WE\rho \propto W\rho^{\zeta+1}T^{\xi} \tag{5}$$

The distribution of J, normalized by its maximum value, is shown in Fig. 3 for both configurations. The effect of the difference in the temperature distributions is clearly evident; the maximum radiation occurs at smaller values of y/y_e for a boundary layer on a cone as contrasted to that on a blunt body. Furthermore, because of the positive value of the density exponent ζ, the maximum of the polyethylene radiation is shifted toward the wall for both geometries. The maximum level of J is indicated for each case. Since the areas under each curve are approximately equal, the heating flux per unit area for equal-thickness boundary layers is approximately proportional to J_{max}. Thus, it can be seen that the local ablation-products radiation to the surface will be a factor of 5 to 10 higher (for polycarbonate and polyethylene, respectively) for the blunt body at equal flight conditions and at equal y_e. However, y_e increases from zero as $x^{1/2}$ for the cone and is essentially constant for the blunt body. For the preceding case, with the additional condition of base diameters of 1 cm for both geometries, the total ablation-products radiation flux $\dot{Q}_a$ is calculated as approximately a factor of 10 to 20 higher (polycarbonate and polyethylene, respectively) for the blunt body than for the cone.

The final form of Eq. (2) for a boundary layer on a conical body, as developed in the Appendix, is

$$\dot{Q}_a = \left(\frac{4\pi}{5(6)^{1/2}}\right)\frac{K\rho_e^{\zeta+1}T_e^{\xi}W_w \sin\theta_c x_b^{3}}{Re^{1/2}l_e^{1/2}}\int_0^{\eta_e}\left(\frac{1-g}{1-g_w}\right)\times\left(\frac{T}{T_e}\right)^{\xi}\left(\frac{\rho}{\rho_e}\right)^{\zeta}d\eta \tag{6}$$

where g is the ratio of local total enthalpy to the edge total enthlapy, Re is the Reynolds number based on slant length,

§ In converting the linear profiles of Ref. 1 to the form of Figs. 2 and 3, it was assumed that the state properties of the mixture boundary layer are those of equilibrium air.

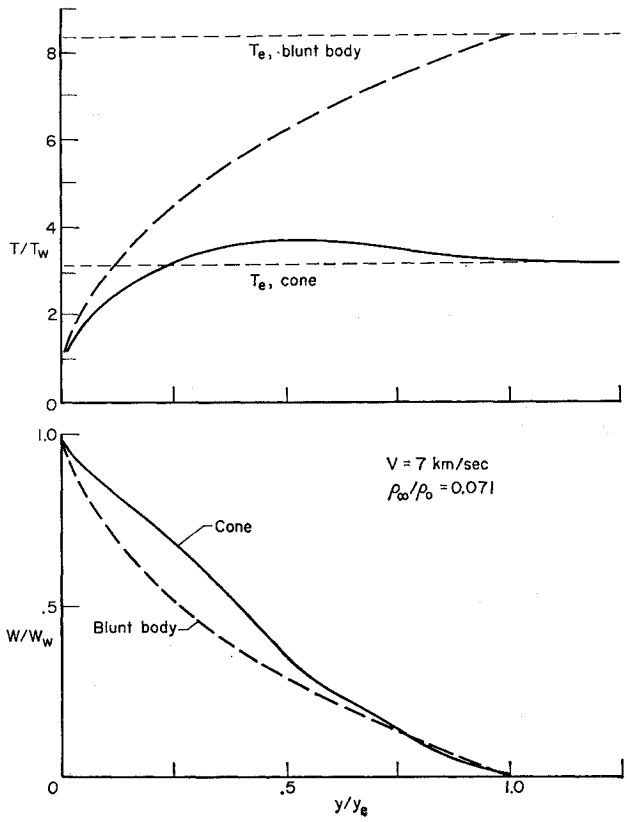

Fig. 2 Boundary-layer profiles of temperature and ablation-products concentration.

$l = \rho\mu/\rho_w\mu_w$, μ is the viscosity, x_b is the slant length of the cone, and η is a transformed normal distance given by

$$\eta = \frac{u_e r}{(2\gamma)^{1/2}}\int_0^y \rho\, dy$$

where

$$\gamma = \int_0^x \rho_w\mu_w u_e r^2\, dx$$

Experiments

A small amount of data on ablation-products radiation from cones was collected for comparison with the results of

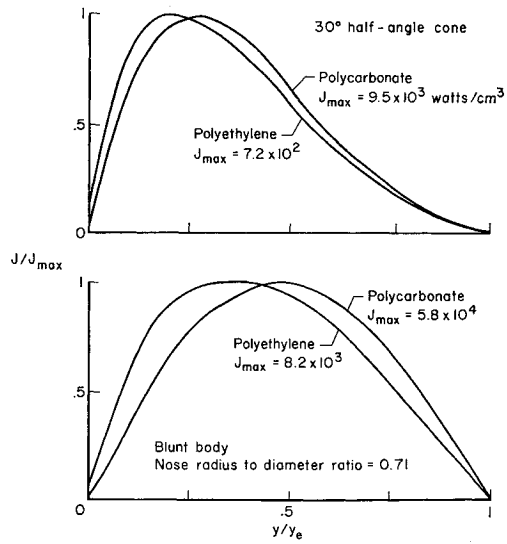

Fig. 3 Profiles of local radiation in the boundary layer; V = 7.0 km/sec, ρ_∞/ρ_0 = 0.071.

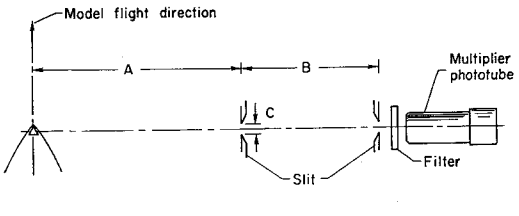

	A	B	C
Blunt nose tests	9 cm	32 cm	1.0 cm
Cone tests	43 cm	38 cm	1.3 cm

Fig. 4 Radiometer geometries.

the analysis. The facility used was the Prototype Hyper velocity Free-Flight Facility of the Ames Research Center.[9] Models were launched by a light-gas gun into a test chamber containing air at various pressures. Radiometers and conventional ballistic-range shadowgraphs spaced along the test chamber provided data on radiant intensity, model velocity, and attitude. The tests covered a freestream density range of 0.007 to 0.13 of sea level and were made at velocities from 6 to 7.2 km/sec.

The models were 30° half-angle cones with a base diameter of 1 cm. The ablating models were made of polyethylene and polycarbonate (trade name, Lexan). Calculations showed that these models always traveled at least 10 times the distance required for the surface temperatures to attain that temperature necessary for ablation before the models reached the radiometer station, intimating that sufficient time was available to approach steady-state ablation closely. Further calculations and observations of the shadowgraphs showed that the mass loss from these models due to ablation was small enough so that the shape of the models was not appreciably altered during the test. Models made from 7075 T-6 aluminum alloy with a slightly blunted (0.1-mm radius) copper tip were also tested. Both calculations and observations of the shadowgraphs showed that these models did not ablate during the tests. Tests of blunt-nose models were of a similar nature.[1] The blunt-model tests covered a velocity range of 4.5 to 7.5 km/sec.

Eleven narrow-pass (typically 0.04-μ) radiometers were used to determine the spectral intensity of radiation from 0.2 to 1.1 μ. Each radiometer consisted basically of a multiplier phototube, a narrow-pass optical filter, and two slits, as is shown schematically in Fig. 4. Slit width was chosen to allow observation of the radiation from the forebody shock layer without interference from wake radiation. Calibration of the radiometers and the data-reduction procedure are described in detail in Ref. 1.

Data and Data Reduction

Figure 5 shows the general features of radiation about cones. The figure is a photograph of an ablating cone taken with an image-converter camera. The light source was the radiation in the vicinity of the model. The effect of the S-11 spectral response of the image converter and the transmission of the

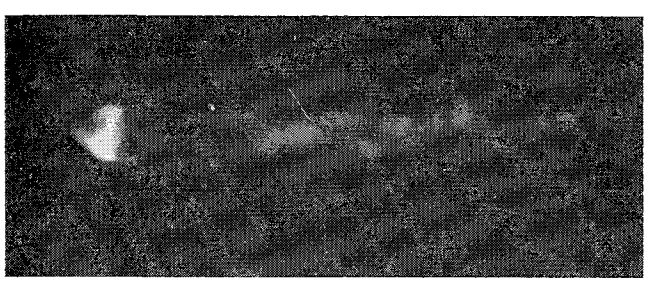

Fig. 5 Image-converter picture of an ablating cone; r_b = 0.51 cm, cone half-angle = 30°, material = polycarbonate, exposure time = 0.5 μsec, V = 6.05 km/sec, ρ_∞/ρ_0 = 0.118, Re = 0.8 × 10^6.

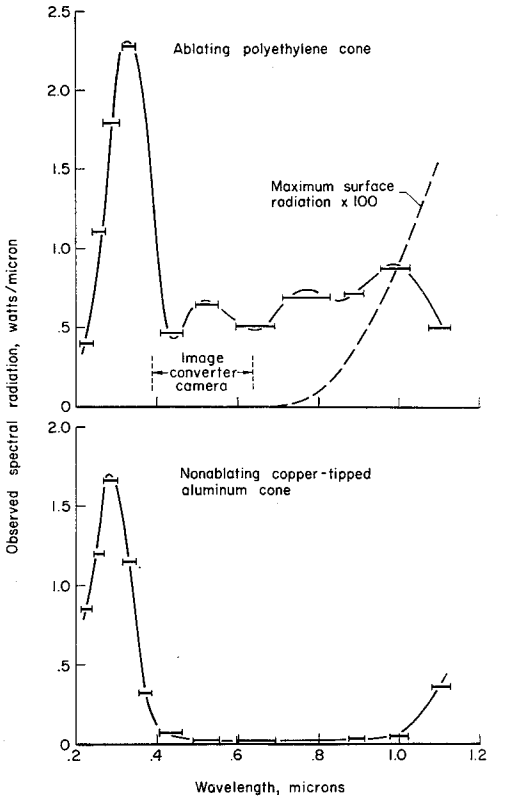

Fig. 6 Examples of spectra; V = 7.0 km/sec, ρ_∞/ρ_0 = 0.013

lens and test-section window limits the responsive wavelength region to 0.39 to 0.65 μ, and, as will be shown later, the major fraction of the radiation which falls into this spectral region is from ablation products. The figure is thus primarily a photograph of the radiating ablation products. The pattern of radiation is not symmetric because of a slight angle of attack.

Figure 6 presents typical spectra of the observed radiation in watts per micron into 4π sr, obtained from ablating and nonablating cones. The ablation material is polyethylene (the same general features are observed in spectra from ablating polycarbonate), and the nonablating model is a copper-tipped aluminum cone. These spectra are constructed by fairing curves through the data which are represented by the horizontal lines whose lengths indicate the 50% bandpass widths of the radiometers. The area under each line indicates total power viewed by each radiometer in its wavelength band. Included for reference is the spectrally responsive region of the image converter used to obtain the photograph presented previously in Fig. 5. For purposes of comparison, the maximum possible surface radiation contribution, multiplied by 100, is also presented in Fig. 6. The calculation of the surface contribution is based on an emissivity of one and a surface temperature of 1000°K.¶ It is apparent from the figure that the contribution of the surface radiation to the total radiation observed is insignificant. Further tests[1] show similar results for blunt bodies. Thus, the spectrum from the ablating model is considered to represent radiation from ablation products and from air in the shock layer, whereas the spectrum from the nonablating model represents radiation from the air in the shock layer alone.[11] It can also

¶ Approximately 1000°K is given for the surface temperature of ablating polyethylene,[10] and T. Wentink Jr., L. Isaacson, and G. Economou of Avco Corporation have recently measured by photometric techniques the same temperature for ablating polycarbonate. The aluminum surface is limited to its melting temperature, 920°K. Hence, the estimate shown is roughly applicable to both types of model materials.

be seen that the ablation-products radiation is generally at wavelengths longer than 0.45 μ. It is apparent that the radiation contributed by the ablation products is comparable to that generated by air in the shock layer. A similar observation was made for blunt models.[1]

The observations of the radiation from the shock layer were converted to ablation-products heating flux $\dot{Q}_a$. To obtain the values of $\dot{Q}_a$ reported in this paper, the spectra were intgerated from 0.45 to 1.1 μ (the same spectral range used in Ref. 1), multiplied by 2 because approximately one-half of the radiation is blocked from view by the model, and then divided by 2 because approximately one-half of the radiant energy is emitted toward the model surface. Ablation-products radiation occurs beyond 1.1 μ[2]; hence, the data herein are considered to be lower limits.

A summary of data from similar blunt-model tests is given in Ref. 1, whereas Table 1 gives a summary of data obtained from the cone-model tests, together with other test parameters. Data were not included from cone tests where the angle of attack was greater than approximately 5°, since ablation-products radiation was found to be sensitive to angle of attack.

Comparison with Data from Cone Models

In this section, the data taken during tests of ablating cones are compared with predictions based upon the preceding analysis. To obtain the predictions, the temperature, density, and enthalpy distributions were calculated for several values of boundary-layer-edge density and freestream velocity. Equation (6) was integrated, and the radiation from both polycarbonate and polyethylene ablation products was calculated for the geometry of the conical test model. The results of the calculations are shown in Fig. 7 as the shaded regions. Here again $\dot{Q}_a$ has been divided by the fourth power of the boundary-layer-edge temperature, as indicated by Eq. (6) for $\xi = 4$. In computing the edge conditions for these predictions, it was assumed that the shock layer was in thermodynamic and chemical equilibrium. The figure shows that, within the framework of the assumptions of the analysis, ablation-products radiation from the boundary layer on a conical model should have the same qualitative features as the radiation from the boundary layer on a blunt model; that is, the general level of the polycarbonate ablation-products radiation is higher than that from polyethylene, whereas the density dependence of polyethylene radiation is larger than that of polycarbonate radiation.

Shown also in Fig. 7 are the ablation-products radiative heating fluxes $\dot{Q}_a$ measuring during cone-model tests. The Reynolds numbers of these tests were never greater than 10^6 based on local flow properties and slant length, so that it is reasonable to expect laminar boundary layers. The data show agreement with the predicted values within a factor of 2. The one exception is a polyethylene data point obtained under low-density conditions such that the air behind the shock wave is noted to be substantially out of equilibrium based on calculations made by D. Eastman and C. Olson of the Boeing Company. The nonequilibrium condition leads to higher boundary-layer temperatures than were used in the predictions, which rely on an equilibrium air assumption; hence, a low predicted value is to be expected in this instance.

Table 1 Summary of Data Obtained from Cone-Model Tests

Ablation material	V, km/sec	ρ_∞/ρ_0	$\dot{Q}_a$, w	ρ_e/ρ_0	Re
Polyethylene	6.88	0.0066	0.2	0.062	0.05×10^6
Polyethylene	7.16	0.066	1.0	0.60	0.5×10^6
Polyethylene	6.91	0.13	1.6	1.2	1.0×10^6
Polyethylene	6.61	0.13	1.4	1.1	1.0×10^6
Polycarbonate	6.05	0.12	30	1.0	0.8×10^6

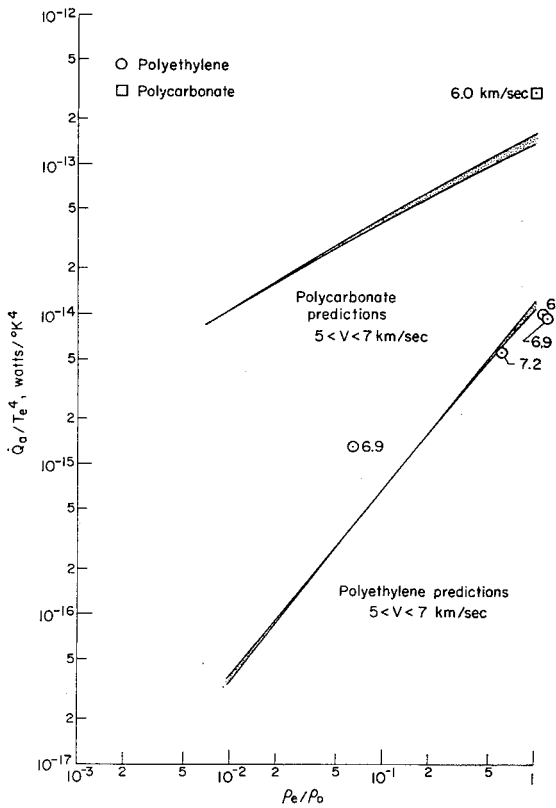

Fig. 7 Comparison of cone data with predictions.

Concluding Remarks

It was shown by ballistic-range experiments performed as part of this study that one of the major components of radiation observed during flight of ablating cones at hypersonic speeds is due to ablation products present in the shock layer. The amount of ablation-products radiation observed is a function of ablation material as well as flight parameters.

A method has been described for predicting the ablation-products radiative heating from the boundary layer of a cone. The method relies on ablation properties deduced from study of a comparable blunt body. Predictions made by this method agree with measured values to within a factor of 2 for the two ablation materials investigated, polyethylene and polycarbonate. This agreement is significant because 1) the distributions of properties in the boundary layer of a cone are significantly different from those in the boundary layer on a blunt body, and 2) the average temperatures and densities in the cone boundary layer for the test conditions are lower by a factor of 2 than those for the blunt-body test conditions.

Because of the agreement between the cone tests and predictions, it appears that ablation-products radiative heating fluxes on bodies of arbitrary shapes can be predicted to at least order-of-magnitude accuracy if the appropriate boundary-layer quantities can be obtained.

Appendix

The radiative heating flux $\dot{Q}_a$ from the ablation products in the boundary layer to the wall is given by Eq. (2) of the text as

$$\dot{Q}_a = \frac{1}{2} \int_{\text{surface}} \int_0^{v_e} WE\rho \, dy \, ds \tag{A1}$$

where

$$E = K\rho^\xi T^\xi \tag{A2}$$

To integrate Eq. (A1) for the case of an ablating cone, W, ρ, and E must be specified in terms of the variable of integra-

tion. Thus, the equations describing the appropriate boundary-layer flow must be formulated and solved.

The major assumptions used in defining the present model of the boundary layer with mass injection on a cone in equilibrium air were the following: 1) the usual thin boundary-layer assumptions; 2) the air state and transport properties are the total properties of the mixture (i.e., they include the chemical reaction terms implicitly); 3) radiative and convective energy coupling is neglected; and 4) the mass injected is gaseous, and the state and transport properties are the same as equilibrium air, with the exception of the radiative property, which is given by Eq. (A2). Under these assumptions, the boundary-layer equations are as follows:

Conservation of Mass

$$(\partial/\partial y)\,(\rho u r) + (\partial/\partial x)\,(\rho v r) = 0 \tag{A3}$$

Conservation of Momentum

$$\rho u \frac{\partial u}{\partial x} + \rho v \frac{\partial u}{\partial y} = \frac{\partial}{\partial y}\left(\mu \frac{\partial u}{\partial y}\right) \tag{A4}$$

Conservation of Energy

$$\rho u \frac{\partial h}{\partial x} + \rho v \frac{\partial h}{\partial y} = \mu \left(\frac{\partial u}{\partial y}\right)^2 + \frac{\partial}{\partial y}\left(\frac{k}{c_p}\frac{\partial h}{\partial y}\right) \tag{A5}$$

Diffusion Equation

$$\rho u \frac{\partial W}{\partial x} + \rho v \frac{\partial W}{\partial y} - \frac{\partial}{\partial y}\left(\rho V_d \frac{\partial W}{\partial y}\right) = 0 \tag{A6}$$

Equation (A5) is more useful if combined with Eq. (A4) and rewritten in terms of the total enthalpy H as

$$\rho u \frac{\partial H}{\partial x} + \rho v \frac{\partial H}{\partial y} = \frac{\partial}{\partial y}\left(\frac{\mu}{\sigma}\frac{\partial H}{\partial y}\right) + \frac{\partial}{\partial y}\left[\mu u\left(1 - \frac{1}{\sigma}\right)\left(\frac{\partial u}{\partial y}\right)\right] \tag{A7}$$

where σ is the Prandtl number. The boundary conditions for these equations are

$$\left.\begin{aligned} &\text{at } y = 0\text{:}\quad u = 0,\ v = v_w,\ H = H_w,\ W = W_w \\ &\text{as } y \to \infty\text{:}\quad u \to u_e,\ H \to H_e,\ W \to 0 \end{aligned}\right\} \tag{A8}$$

The boundary-layer model is now defined by Eqs. (A3, A4, A6, and A7) and boundary conditions (A8).

The conservation equations are not coupled with the diffusion equation because of assumptions 2 and 4. Hence, Eq. (A6) may be solved subsequent to the following solution of the coupled equations (A4) and (A7). The following transformations and variables are used:

Howarth Transformation

$$\eta = \frac{u_e r}{(2\gamma)^{1/2}} \int_0^y \rho\, dy \tag{A9a}$$

Mangler Transformation

$$\gamma = \int_0^y \rho_w \mu_w u_e r^2\, dx \tag{A9b}$$

Dimensionless Dependent Variables

$$f = \int_0^\eta f_\eta\, d\eta \qquad f_\eta = \frac{u}{u_e} \qquad g = \frac{H}{H_e} \tag{A10}$$

where variable subscripts indicate differentiation.

The differential equations transform to

$$(l f_{\eta\eta})_\eta + f f_{\eta\eta} = 2\gamma(f_\eta f_{\eta\gamma} - f_\gamma f_{\eta\eta}) \tag{A11a}$$

$$\left(\frac{l}{\sigma} g_\eta\right)_\eta + f g_\eta + \frac{u_e^2}{H_e}\left[\left(1 - \frac{1}{\sigma}\right) l f_\eta f_{\eta\eta}\right]_\eta = 2\gamma(f_\eta g_\gamma - f_\gamma g_\eta) \tag{A11b}$$

$$\left(\frac{l}{Sc} W_\eta\right)_\eta + f W_\eta = 2\gamma(f_\eta W_\gamma - f_\gamma W_\eta) \tag{A11c}$$

where $l = \rho\mu/\rho_w\mu_w$, $Sc = \mu/\rho V_d$, and the boundary conditions transform to

$$\left.\begin{aligned} &\text{at } \eta = 0\text{:}\quad f_\eta = 0, f = f_w, g = g_w, W = W_w \\ &\text{as } \eta \to \infty\text{:}\quad f_\eta \to 1, g \to 1, W \to 0 \end{aligned}\right\} \tag{A12}$$

A stream function ψ defined to satisfy Eq. (A3) is given by

$$\partial\psi/\partial y = \rho u r \qquad -(\partial\psi/\partial x) = \rho v r$$

and is used together with Eq. (A10) to obtain the value of f at the wall, the blowing parameter. The result is

$$f_w = \left[\int_0^x \dot{m}(x) r\, dx \Big/ (2\gamma)^{1/2}\right] \tag{A13}$$

where $\dot{m}(x) = \rho_w v_w$ and is the rate of mass injection. For a simple ablation process, the wall temperature is taken as constant, and $\dot{m}$ is given by

$$\dot{m}(x) = \dot{q}_c(x)/h_{\text{eff}} \tag{A14}$$

where h_{eff} is the effective heat of ablation (assumed to be independent of heating rate) and $\dot{q}_c(x)$ is the cold-wall convective heating with zero mass injection** and is given by, for the case of a cone,

$$\dot{q}_c(x) = K_c(\rho_e, \theta_c, V, T_w)/x^{1/2} \tag{A15}$$

The zero mass injection heating rates as calculated from solutions of (A11a) and (A11b) are given in Ref. 12. For example, $\dot{q}_c(x)$ for a 30° half-angle cone with a wall temperature of 1000°K is given by

$$\dot{q}_c(x) = 0.704 \frac{k_w}{c_{p_w}}\left(\frac{\rho_w u_e x}{\mu_w}\right)^{1/2} \frac{1}{x}(H_e - H_w)V^{-0.36} \tag{A16}$$

where the units of the coefficient 0.704 are $(\text{km/sec})^{0.36}$. The effective heats of ablation, as reported in Ref. 13, are

$$\left.\begin{aligned} &\text{Polyethylene} \\ &\qquad h_{\text{eff}} = 4660 \text{ joules/g} + 0.5(H_e - H_w) \\ &\text{Polycarbonate} \\ &\qquad h_{\text{eff}} = 2910 \text{ joules/g} + 0.5(H_e - H_w) \end{aligned}\right\} \tag{A17}$$

It is easily shown that f_w is not a function of x. This result, together with the isothermal wall assumption and the equilibrium air assumptions, allows the right-hand sides of Eqs. (A11) to be set to zero (i.e., similarity holds).

The relations resulting from setting equations (A11a) and (A11b) to zero were programed and solved on a digital computer by a fourth-order Adams-Moulton procedure.[14] The equilibrium air properties, as correlated in Ref. 15, were used. Profiles of boundary-layer properties were generated, and a typical temperature profile is shown in Fig. 2. This figure shows the characteristic overshoot of temperature in the boundary layer of a cone.

Before Eq. (A1) is integrated, the mass concentration must be specified. This can be obtained by integration of Eq. (A11c), the transformed diffusion equation. However, a simple approximation, consistent with the degree of approximations used in obtaining the empirical constants in Eq. (A2), is obtained when we use the Crocco result, namely, $Sc = 1$ and $\sigma = 1$. We can then write the ablation-products mass fraction as

$$W = W_w\,[(1 - g)/(1 - g_w)] \tag{A18}$$

which can be verified by substitution into Eq. (A11c) and comparison with Eq. (A11b). A similar approach could have been used to solve the transformed continuity equations, but the effect of setting the Prandtl number equal to unity

** The present analysis is based on convective heating. More generally, if other heating sources are to be considered, the equation for $\dot{m}(x)$ would be suitably modified.

would reduce or eliminate the overshoot in temperature. Since ablation-products radiation is sensitive to the temperature (about as T^4), this profile change could result in significant error in the evaluation of Eq. (A1). The ablation-products mass fraction at the wall, required for analytical formulation of Eq. (A18), can be obtained if the net flow of air at the wall is zero. Analytically,

$$\rho_w V_d(\partial W/\partial y)_w + \rho_w v_w(1 - W_w) = 0 \qquad \text{(A19)}$$

which transforms to

$$W_{\eta w} = (Sc) f_w(1 - W_w) \qquad \text{(A20)}$$

and can be solved by integration of Eq. (A11c) twice using Eqs. (A11b) and (A19) with boundary conditions (A12). The result is

$$W_w = \left(1 - \left\{\frac{(f_{\eta\eta w})^{Sc}}{Scf_w \int_0^\infty \left[\frac{(lf_{\eta\eta})^{Sc}}{l}\right] d\eta}\right\}\right)^{-1} \qquad \text{(A21)}$$

Using the assumption $Sc = 1$ reduces (A21) to

$$W_w = 1/[1 - (f_{\eta\eta w}/f_w)] \qquad \text{(A22)}$$

We note that W_w is a function of the blowing parameter f_w and the shear stress parameter $f_{\eta\eta w}$. The shear stress parameter is obtained from solution of Eqs. (A11a) and (A11b).

The total ablation-products radiation heating flux may now be calculated from Eq. (A1), which is integrated once and transformed to yield

$$\dot{Q}_a = \left(\frac{4\pi}{5(6)^{1/2}}\right) \frac{K\rho_e{}^{\xi+1} T_e{}^{\xi} W_w \sin\theta_c x_b{}^3}{Re^{1/2} l_e{}^{1/2}} \int_0^{\eta_e} \left(\frac{1-g}{1-g_w}\right) \times \left(\frac{\rho}{\rho_e}\right)^{\xi} \left(\frac{T}{T_e}\right)^{\xi} d\eta \qquad \text{(A23)}$$

where

$$Re = \rho_e u_e x_b/\mu_e.$$

References

[1] Craig, R. A. and Davy, W. C., "Thermal radiation from ablation products injected into a hypersonic shock layer," NASA TN D-1978 (1963).

[3] Steinberg, M., Maiden, C. J., Leak, W. R., and Hansen, C. F., "Preliminary studies of the effects of ablation contaminants on radiation," General Motors Defense Research Lab. Rept. TR62-209H (1962).

[3] Canning, T. N. and Page, W. A., "Measurements of radiation from flow fields of bodies flying at speeds up to 13.4 kilometers per second," AGARD Fluid Mechanics Panel (April 3–6, 1962).

[4] Lemay, A., "Radiation measurements from the plasma sheath surrounding hypersonic projectiles," Canadian Armament Research and Development Establishment TM 693/62 (1962).

[5] Leverance, R. A., "A comparison of the visible radiation from projectile materials at velocities from 6000 to 8500 ft/sec," Naval Ordnance Lab. 61-162 (1961).

[6] Allen, H. J., Seiff, A., and Winovich, W., "Aeroydnamic heating of conical entry vehicles at speeds in excess of earth parabolic speed," NASA TR R-185 (1963).

[7] Schlichting, H., *Boundary Layer Theory* (McGraw-Hill Book Co., Inc., New York, 1955).

[8] Hansen, C. F., "Approximations for the thermodynamic and transport properties of high temperature air," NASA TR R-50 (1959).

[9] Seiff, A., "Ames hypervelocity free-flight research," Astronaut. Aerospace Eng. **1**, 60 (December 1963).

[10] Vojovodich, N. S., "The performance of ablative materials in a high-energy, partially dissociated, frozen nitrogen stream," NASA TN D-1205 (1962).

[11] Compton, D. L. and Cooper, D. M., "Measurements of radiative heating on sharp cones," AIAA Preprint 64-252 (June 1964).

[12] Canning, T. N., "Physics of hypervelocity flight as it affects the design of re-entry vehicles," *Proceedings of the Ninth Anglo-American Conference* (American Institute of Aeronautics and Astronautics, New York, to be published).

[13] Savin, R. C., Gloria, H. R., and Dahms, R. G., "The determination of ablative properties of materials in free-flight ranges," NASA TN D-1330 (1962).

[14] Hildebrand, F. B., *Introduction to Numerical Analysis* (McGraw-Hill Book Co., Inc., New York, 1956), Chap. 6.

[15] Viegas, J. R. and Howe, J. T., "Thermodynamic and transport property correlation formulas for equilibrium air from 1000°K to 15,000°K," NASA TN D-1429 (1962).